arXiv:2208.07174v3 [cs.RO] 21 Aug 2023

A Man-in-the-Middle Attack against Object Detection Systems

Han Wu, Sareh Rowlands and Johan Wahlström

***Abstract*—Object detection systems using deep learning models have become increasingly popular in robotics thanks to the rising power of CPUs and GPUs in embedded systems. However, these models are susceptible to adversarial attacks. While some attacks are limited by strict assumptions on access to the detection system, we propose a novel hardware attack inspired by Man-in-the-Middle attacks in cryptography. This attack generates an Universal Adversarial Perturbation (UAP) and then inject the perturbation between the USB camera and the detection system via a hardware attack. Besides, prior research is misled by an evaluation metric that measures the model accuracy rather than the attack performance. In combination with our proposed evaluation metrics, we significantly increases the strength of adversarial perturbations. These findings raise serious concerns for applications of deep learning models in safety-critical systems, such as autonomous driving.**

***Impact Statement*—Advancements in deep neural networks have ushered in a new era of robotics, characterized by intelligent robots with a comprehensive understanding of the environment, thanks to deep learning models. However, it is no more a secret that deep learning models are vulnerable to adversarial attacks. Besides existing digital and physical attacks, we introduce a novel 'Man-in-the-Middle' hardware attack that injects digital perturbation into the physical sensor. Our research opens up new possibilities for adversarial attacks, and we hope to embrace deep learning models securely for robotic applications.**

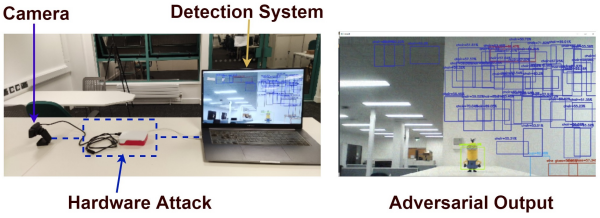
***Index Terms*—Adversarial Attacks, Object Detection, Deep Learning.**



(a) Man-in-the-Middle Attack in Network Security



(b) Man-in-the-Middle Attack in Deep Learning



(c) Demo of the Hardware Attack

Fig. 1: The Man-in-the-Middle hardware attack.

I. Introduction

The development of deep neural networks has enabled the creation of intelligent robots that possess a more comprehensive perception of the environment than traditional robots. However, this shift towards intelligent robots has also brought with it an increasing risk of adversarial attacks, especially in safety-critical applications. It has been nearly a decade since the first adversarial attack against neural networks, in which Goodfellow et al. fooled an image classification model by adding a small perturbation to the input image [1]. Although the perturbation was imperceptible to humans, it caused the deep learning model to produce erroneous classification results. The attack was later extended from classification models to detection models [2], [3].

Adversarial attacks against deep learning models can be divided into two categories: digital attacks and physical attacks. Digital attacks directly apply perturbations to the digital input image by modifying pixel values [4], while physical attacks involve printing the perturbation on physical objects such as posters [5] or T-shirts [6].

Han Wu, Sareh Rowlands and Johan Wahlström are currently with the University of Exeter, Stocker Rd, Exeter EX4 4PY UK (e-mail: hw630@exeter.ac.uk; s.rowlands@exeter.ac.uk; j.wahlstrom@exeter.ac.uk).

However, both digital and physical attacks have their limitations. Digital perturbation requires access to the detection system, making it difficult to apply in real-world scenarios such as hacking into a self-driving car. Physical attacks, on the other hand, are sensitive to position and angle variations. For instance, experiments in [3] showed that an autonomous vehicle only misclassified traffic signs placed within 0.5 meters of the camera and viewed from specific angles. Moreover, these attacks lack flexibility, as once the adversarial object is printed, it can only be changed through reprinting. The trial-and-error process of finding a successful attack object can take a long time and require significant amounts of printing.

A. Contributions

This paper presents a novel hardware attack that combines the flexibility of physical attacks with the efficiency of digital attacks, inspired by Man-in-the-Middle Attacks in network security (refer to Fig. 1a). In this attack, the adversary intercepts and manipulates the image data transmitted between a USB camera and a detection system (refer to Figs. 1b and 1c).

The key contributions of this research are summarized as follows:

1) We present a novel hardware attack, called Man-in-the-Middle attack, that offers both efficiency and ease of deployment for adversarial attacks[1]. By utilizing learning rate decay during the generation of the perturbation, our attack is capable of generating more bounding boxes than competing attack methods.
2) We introduce three new evaluation metrics that offer a more nuanced approach to evaluating adversarial attacks. Unlike existing metrics that make a binary decision for each bounding box, our metrics consider the confidence value and probability vector in a linear fashion.
3) We devise and open source the white-box adversarial toolbox[2] that simplifies the process of generating adversarial perturbations. The toolbox focuses on real-time white-box attacks against object detection models.

II. Preliminaries

A. Object Detection Models

The task of object detection aims to locate the position and classify the category of each object in an image. Therefore, the task consists of two distinct problems: localization and classification. Existing object detection models can be categorized into two types, one-stage and two-stage methods, based on whether these two problems are solved together or separately [7]. Two of the most widely deployed one-stage models are YOLO [8], [9], [10] and SSD [11], which can achieve real-time performance on CPUs without GPUs. Faster RCNN [12] and Mask RCNN [13] are two well-known two-stage models.

In robotic applications, one-stage models are generally preferred due to their speed and acceptable accuracy in most situations. In this study, we investigate how these attacks affect real-time robotic applications and focus on energy-efficient one-stage models.

B. Adversarial Attacks

The Fast Gradient Sign Method (FGSM) [1] was the first adversarial attack against classification models, using gradients to generate image-specific perturbations. However, for real-world robotic applications, it is more practical to use Universal Adversarial Perturbations (UAPs) [14], which are image-agnostic. UAPs demonstrated the ability to fool classification models on most images in a dataset using a single perturbation. Adversarial attacks have since been extended from image classification to detection models [15], [2].

In addition to image-specific and image-agnostic methods, it is also possible to classify adversarial attacks into data-driven and data-independent approaches. Data-driven approaches require access to the input image, while data-independent methods only need access to the parameters and architecture of the target model. Generally, data-driven approaches achieve a higher fooling rate as they have more information at their disposal. Data-driven methods include gradient-based methods [16], [17], [18], [19], methods using Generative Adversarial Networks (GANs) [20], [21], and optimization-based methods [22], [23].

[1]The source code of the hardware attack is available on GitHub: https://github.com/wuhanstudio/adversarial-camera

[2]The source code of the toolbox is available on GitHub: https://github.com/wuhanstudio/whitebox-adversarial-toolbox

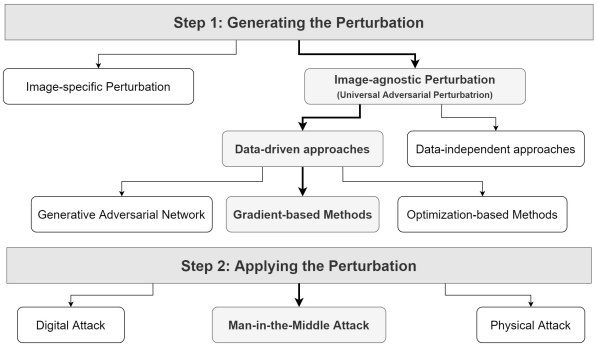


Fig. 2: Our approach to generate and apply adversarial perturbations in bold.

Our proposed method is a gradient-based data-driven approach that generates image-agnostic Universal Adversarial Perturbations (UAPs) and applies them via a Man-in-the-Middle attack, as depicted in Fig. 2.

III. The Man-in-the-Middle Attack

This section introduces the PCB attack, a novel gradient-based method designed to generate image-agnostic UAPs. The name "PCB" comes from the fact that the output of the object detection model is separated into three components: probability vector (P), confidence value (C), and bounding boxes (B). The perturbation is then applied using a Man-in-the-Middle hardware attack. The acronym PCB is fitting for a hardware attack, as it is also used to refer to Printed Circuit Boards (PCB).

A. Problem Formulation

In Section II, we discussed that object detection models can be categorized into one-stage models (e.g., YOLO, SSD) and two-stage models (e.g., Faster-RCNN, Mask-RCNN). Despite the differences in their structures, all these models share common inputs and outputs. To describe these inputs and outputs, we introduce the following mathematical notation:

- x: The original clean input image.
- δ: The adversarial perturbation.
- $x^{'}$: The adversarial input image $x^{'} = x + \delta$.
- K: The total number of candidate classes.
- N: The total number of candidate bounding boxes.
- $\mathcal{O}(x)$: The output of N candidate bounding boxes from the model given the input image x.
- $o_i(x)$: The i_{th} output in $\mathcal{O}(x) = \{o_1, o_2, o_3, ..., o_N\}$, where $o_i = (b_i, c_i, p_i)$. $1 \leq i \leq N$.
- b_i: The location and dimension of the i_{th} candidate box. $b_i = (b_i^x, b_i^y, b_i^w, b_i^h)$ represents a bounding box at position (b_i^x, b_i^y) with width b_i^w and height b_i^h,
- c_i: The confidence value (objectness) of the i_{th} candidate box that represents how probable it is that the the candidate box represents an object.
- p_i: The softmax probability vector of the i_{th} candidate box. $p_i = (p_i^1, p_i^2, ..., p_i^K)$ for K classes and $\sum p_i = 1$.

Given an input image x, the object detection model outputs N candidate bounding boxes $\mathcal{O}(x) = \{o_1, o_2, o_3, ..., o_N\}$. Each candidate box $o_i = (b_i, c_i, p_i)$ contains $b_i = (b_i^x, b_i^y, b_i^w, b_i^h)$ that represents the location and dimension of the box, the confidence value $c_i \in [0, 1]$ that represents how probable it is that the the candidate box represents an object, and the softmax probability vector, $p_i = (p_i^1, p_i^2, ..., K_i)$ for K classes. The raw outputs from the detection model $\mathcal{O}(x)$ may contain several thousand candidate bounding boxes. We then use the Non-maximum Suppression (NMS) method [24] to filter out bounding boxes with low confidence values, and high Intersection over Union (IoU) to generate final detection results.

An adversarial example $x^{'} = x + \delta$ aims to fool the detection model by making it output candidate boxes $\mathcal{O}(x^{'})$ that are different from the candidate boxes $\mathcal{O}(x)$ outputted by the model for the original input image x. For example, the adversarial output $\mathcal{O}(x^{'})$ may detect more false positive objects after the non-maximum suppression (NMS) process. To achieve this, we need to generate a perturbation δ that can be added to the original image x to produce the adversarial image $x^{'}$. In the following subsections, we will describe how to generate the perturbation δ using the proposed PCB attack.

B. Generating the perturbation (The PCB Attack)

Gradient-based methods use a similar approach to generate both image-specific and image-agnostic perturbations. For image-specific perturbations, given an input image, the method iterates over a single image to produce the perturbation. For image-agnostic perturbations, given the entire dataset, the method iterates over multiple images to generate the Universal Adversarial Perturbation (UAP). We will first describe how we generate the image-specific perturbations and then extend the attack to generate the image-agnostic perturbations.

1) ***Image-specific PCB Attack****:* The intuition behind gradient-based methods is straightforward. During the training process, we minimize the training loss

$$\min_{\mathcal{W}} \ \mathcal{L}_{train} = f(\mathcal{W}; x, \mathcal{O}) \tag{1}$$

by updating the model weights. Note that the training loss is a function of the input x, the model weights $\mathcal{W}$, and the ground truth $\mathcal{O}$.

However, our objective is to fool the detection model to make inaccurate predictions. Therefore, during the attack, we maximize the adversarial loss

$$\max_{x} \ \mathcal{L}_{adv} = f(x; \mathcal{O}^*, \mathcal{W}) \tag{2}$$

by updating the input x and using the desired adversarial outputs $\mathcal{O}^*$. Different gradient-based methods use different adversarial loss functions $\mathcal{L}_{adv}$ and construct desired adversarial outputs $\mathcal{O}^*$ differently. In our attack, we separate the Probability vector and Confidence value (PC) with Bounding boxes (B) and investigate the two adversarial loss functions

$$\mathcal{L}_{PC}(x) = \sum \sigma(c_i) * \sigma(p_i) \tag{3}$$

and

$$\mathcal{L}_{PCB}(x) = \frac{\sum (\sigma(c_i) * \sigma(p_i)}{\sum [\sigma(w_i) * \sigma(h_i)]^2}. \tag{4}$$

Using $\mathcal{L}_{PCB}(x)$ will give smaller bounding boxes, while $\mathcal{L}_{PC}(x)$ gives larger bounding boxes. By maximizing the adversarial loss, we generate large amounts of incorrect bounding boxes (fabrication attack). By minimizing the loss, we remove bounding boxes (vanishing attack).

The optimization of (2) is performed by first zero-initializing the perturbation δ, and then using Projected Gradient Descent (PGD) [25] with learning rate decay so that

$$\delta_{t+1} = proj_p(\delta_t + \alpha sign(\frac{\partial L_{adv}(x_t'; O^*)}{\partial x_t'})). \tag{5}$$

The image-specific PCB attack is summarized in Algorithm 1, where $\texttt{proj}_\infty(\delta, \epsilon)$ is the projection function $\min(\delta, \epsilon)$ and $\texttt{clip}(-1, 1)$ is the unit clip function.

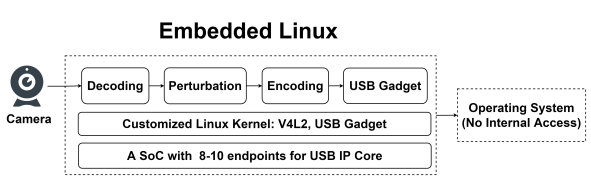
Algorithm 1 Image-specific PCB Attack

Input: The target model, the input image x.
Parameters: The learning rate α, learning rate decay k, number of iterations n, and strength of the attack ϵ.
Output: Image-specific perturbation δ
Initialize $\delta \leftarrow 0$
for $i = 1 : n$ **do**
  $x^{'} = x + \delta$
  $\nabla = \frac{\partial L^*_{adv}(x'; O^*)}{\partial x^{'}}$
  $\delta \leftarrow \delta + \alpha * \texttt{sign}(\nabla)$
  $\delta \leftarrow \texttt{clip}(-1, 1)$
  $\delta \leftarrow \texttt{proj}_\infty(\delta, \epsilon)$
  // Learning Rate Decay*
  $\alpha = \alpha * k$
end for

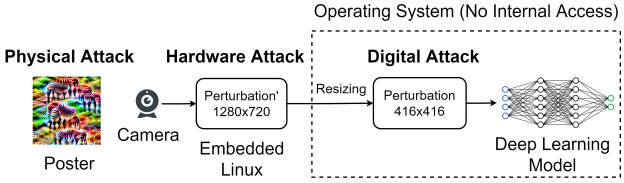
Algorithm 2 Image-agnostic PCB Attack (UAP)

Input: The target model, the sample images X_S.
Parameters: The learning rate α, learning rate decay k, number of iterations n, and strength of the attack ϵ.
Output: Image-specific perturbation δ
Initialize $\delta \leftarrow 0$
for $i = 1 : n$ **do**
  for each image $x \in X_s$ **do**
    $x^{'} = x + \delta$
    $\nabla = \frac{\partial L_{adv}(x^{'})}{\partial x^{'}}$
    $\delta \leftarrow \delta + \alpha * \texttt{sign}(\nabla)$
    $\delta \leftarrow \texttt{clip}(-1, 1)$
    $\delta \leftarrow \texttt{proj_p}(\delta,\ \epsilon)$
  end for
  // Learning Rate Decay*
  $\alpha = \alpha * k$
end for

2) ***Image-agnostic PCB Attack****:* We can extend the method to an image-agnostic attack by iterating over a collection of images $X_s = x_1, x_2, ..., x_n$, where n is the number of available images to the attacker. X_s can be thought of as the training set or a video clip from the target scene. Initially, we generate a random or zero-initialized perturbation δ that is of the same dimension as the input of the detection model.



(a) The Design of the Embedded System.



(b) The Physical Attack, Hardware Attack and Digital Attack.

Fig. 3: The system design architecture of the Man-in-the-Middle hardware attack, as well as its differences from physical attacks and digital attacks.

In each iteration, we update δ using the gradient of input with respect to $\mathcal{L}_{adv}$. The learning rate α is relatively small compared to the image-specific PCB attack to ensure that the perturbation is universal across images. We summarize the image-agnostic PCB attack in algorithm 2.

C. Applying the perturbation (The Man-in-the-Middle Attack)

In Section I, we mentioned that conducting digital attacks can be challenging due to the lack of access to the internal system. Input images are often resized and processed by intermediate components before being fed into the detection system. Therefore, an attacker needs to penetrate the operating system and inject malicious code into the embedded system.

To address this problem, the Man-in-the-Middle hardware attack was developed. By eavesdropping and manipulating the image data before it reaches the detection system, the perturbation can be applied without access to the operating system.

To implement the Man-in-the-Middle hardware attack, specialized hardware such as Raspberry Pi Zero/4 or I.MX6UL is required, which can read raw images from the USB camera and then inject the perturbation (see Fig. 3). To conceal the attack from the operating system, a virtual camera needs to be simulated to the detection system. This requires a Linux kernel that supports the V4L2 driver, the USB gadget framework, and configfs.



(a) The mAP cannot distinguish between fabrication and vanishing attacks (both mAP = 0).



(b) The mAP does not consider confidence values (both mAP = 0).

Fig. 4: The limitations of Mean Average Precision (mAP).

IV. Experimental Evaluation

This section aims to provide insight into why the Mean Average Precision (mAP) not suitable for evaluating adversarial attacks. For adversarial attacks, the choice of the adversarial loss function determines the type of attack to be conducted (e.g., fabrication or vanishing), whereas the strength of the attack is determined by the iteration process. In this study, we employ our novel evaluation metrics to investigate the iteration process and achieve more efficient attacks against a one-stage detection model, namely YOLO, on the VOC2012 dataset [26].

A. Evaluation Metrics

The mAP [27] is typically used to both to measure the accuracy of object detection models and to evaluate the strength of adversarial attacks. However, it can be noticed that the mAP cannot distinguish between different attacks.

For example, both the fabrication and vanishing attacks result in an mAP $\approx$ 0, even though they serve different attacking purposes (see Fig. 4a). Similarly, while an attacker will prefer a stronger attack (Dog 99%) over a weaker attack (Dog 60%), mAP does not reflect the strength of an attack (see Fig. 4b). In addition, note that the overall detection error

$$\begin{aligned} \mathcal{O}(x^{'}) - \mathcal{O}_{true} &= [\mathcal{O}(x^{'}) - \mathcal{O}(x)] + [\mathcal{O}(x) - \mathcal{O}_{true}] \\ &= \boldsymbol{\varepsilon_{\texttt{attack}}} + \varepsilon_{\texttt{model}}, \end{aligned} \tag{6}$$

where $\mathcal{O}_{true}$ is the ground truth model output, includes the attack error $\varepsilon_{\texttt{attack}}$ and the model error $\varepsilon_{\texttt{model}}$. The mAP measures the overall error by comparing the adversarial outputs with the ground truth, but we are only interested in the attack error $\varepsilon_{\texttt{attack}} = \mathcal{O}(x^{'}) - \mathcal{O}(x)$. Therefore, we devise three new evaluation metrics.

1) Mean Confidence Variation: The average increase or decrease of the confidence value of all the bounding boxes at each iteration step t. This metric reflects the strength of the attack on the confidence value and is expressed as $\frac{1}{N}\sum_{i=1}^{N}(c_{t,i} - c_{t-1,i})$.
2) Number of Boxes: The total number of bounding boxes after the NMS. This metric shows how many objects are detected at each step of the attack $|\texttt{NMS}(O(x^{'}))|$.
3) Relative Box Variation: After each iteration, the position of false positive bounding boxes fluctuates. This metric measures the percentage of consistent bounding boxes (bounding boxes that have the same position as in the previous step) at the current step and can be expressed as $\frac{|\texttt{NMS}(\mathcal{O}(x_t^{'}))| + |\texttt{NMS}(\mathcal{O}(x_{t-1}^{'}))| - |\texttt{NMS}(\mathcal{O}(x_t^{'}),\ \mathcal{O}(x_{t-1}^{'}))|}{|\texttt{NMS}(\mathcal{O}(x_t^{'}))|}$.

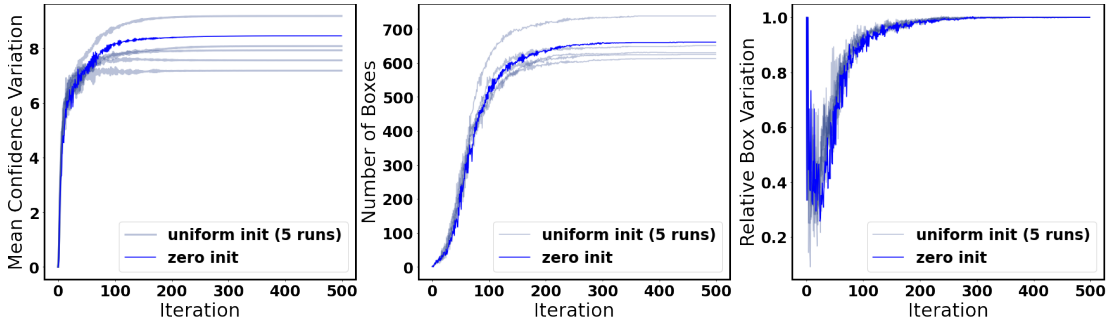


Fig. 5: The PCB fabrication attack using different initialization methods.

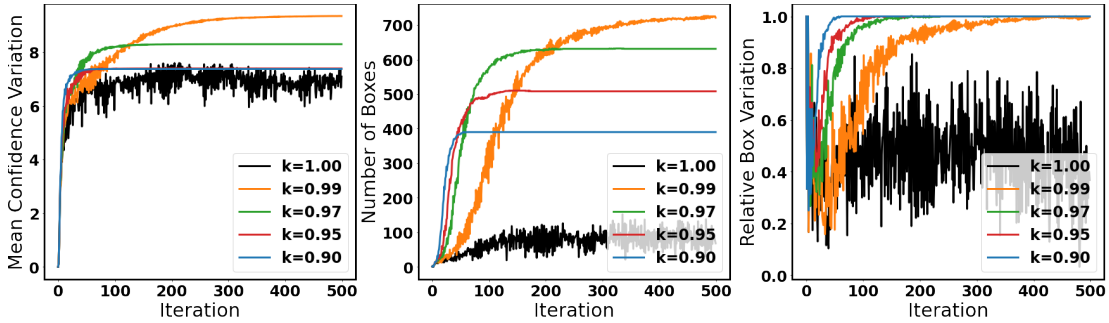


Fig. 6: The PCB fabrication attack with different learning rate decays.

B. Initialization Methods

The TOG attack employs uniform initialization as noted in [16]. In contrast, other attacks use zero initialization, including [28], [17], [18], [25].

Gradient-based attacks rely on gradients to iterate from the original image to an adversarial input. The use of uniform initialization may impede the initial gradient at the first iteration, potentially limiting the attack's effectiveness. To investigate this hypothesis, we conducted 5 runs of the PCB attack with uniform initialization and compared the results with zero initialization. Our evaluation metrics included the mean confidence variation, number of boxes, and relative box variation.

Our results showed that, for the first two evaluation metrics, only one out of five runs with uniform initialization resulted in a more effective attack than zero initialization. This supports our hypothesis that uniform initialization can impede the initial gradient and hinder the attack's effectiveness. Regarding the third evaluation metric, relative box variation, we observed convergence to 1 for both initialization methods, indicating that all false positive bounding boxes were stable, and the convergence speed was similar for both initialization methods.

C. Learning Rate Decay

To achieve a stable and efficient adversarial attack, it is necessary to avoid gradient counteraction, which can cause the attack to vary significantly over iterations. The PCB attack addresses this issue by introducing the learning rate decay factor k, which helps to stabilize the attack over different iterations.

In contrast, the original PGD attack does not use learning rate decay and thus has an unstable iteration process (as shown by the black line in Fig. 6). This issue has not been thoroughly studied in prior research, which has primarily relied on mAP as the evaluation metric. For example, at each step, we generate different false positive bounding boxes at various positions, but none of them matches the ground truth (mAP$=0$). As a result, even though the location of bounding boxes varies a lot (unstable) from one iteration to the next, the mAP stables at 0 which does not indicate unstability of the iteration process.

Using our new evaluation metrics, we can observe the complete iteration process (as depicted in Fig. 6). As the learning rate decay factor k decreases from 0.99 to 0.90, more iterations are required before the two evaluation metrics, the mean confidence variation and the number of boxes, converge. However, both metrics converge at higher values when k decreases, indicating a more efficient attack. Thus, we can conclude that learning rate decay is an effective technique for achieving efficient adversarial attacks.

D. Adversarial Loss Function

In this section, we aim to compare the effectiveness of three different adversarial loss functions for the fabrication attack. Rather than determining the best loss function, our goal is to use our evaluation metrics to highlight the advantages and disadvantages of each method.

As shown in Fig. 7, we observe that the Relative Box Variation of all three methods converges to 1, indicating that the locations of most bounding boxes are stable in the final iterations. Though the PC attack generates the most bounding boxes and achieves the highest Mean Confidence Variation when $k = 0.99$, it requires a larger number of iterations to reach the plateau, which can be computationally expensive when the number of sample images X_s is large.

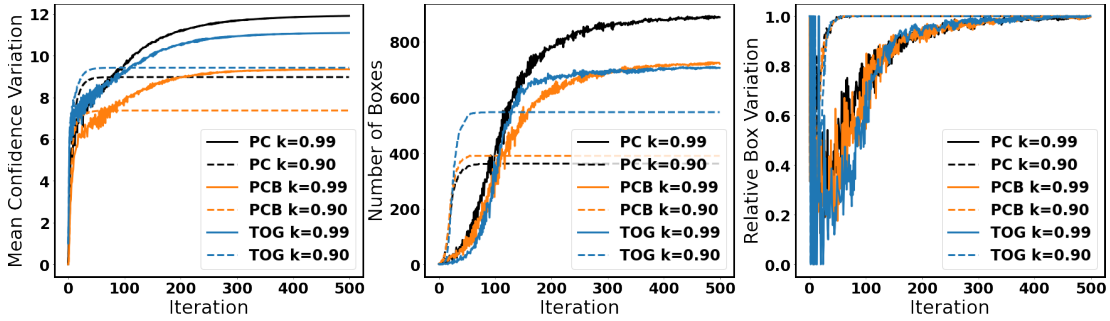


Fig. 7: Different adversarial loss functions of the fabrication attack.

In contrast, both the TOG and PCB attacks converge faster and perform better than the PC attack when $k = 0.90$. Therefore, we cannot definitively state that one method is superior to the others. Instead, the newly proposed evaluation metrics provide useful references for decision-making.

V. Conclusions

This paper presents a novel hardware attack that reveals a previously unknown vulnerability of deep learning object detection systems, posing serious threats to safety-critical applications. Unlike existing attack frameworks, our approach does not rely on any assumption about access to the object detection system, but rather leverages perturbations injected at the hardware level. Our experiments on the VOC2012 dataset and the YOLO detection model demonstrate the high efficiency of our attack. Further research may explore the extension of the attack to other tasks beyond object detection, or to other sensors, such as Lidar.

References

[1] I. Goodfellow, J. Shlens, and C. Szegedy, "Explaining and harnessing adversarial examples," in *International Conference on Learning Representations (ICLR)*, 2015.

[2] H. Wu, S. Yunas, S. Rowlands, W. Ruan, and J. Wahlström, "Adversarial detection: Attacking object detection in real time," in *IEEE Intelligent Vehicles Symposium (IV)*, 2023, pp. 1–7.

[3] J. Lu, H. Sibai, E. Fabry, and D. A. Forsyth, "No need to worry about adversarial examples in object detection in autonomous vehicles," in *IEEE Conference on Computer Vision and Pattern Recognition (CVPR)*, 2017.

[4] H. Wu, S. Yunas, S. Rowlands, W. Ruan, and J. Wahlström, "Adversarial driving: Attacking end-to-end autonomous driving," in *IEEE Intelligent Vehicles Symposium (IV)*, 2023, pp. 1–7.

[5] M. Lee and Z. Kolter, "On physical adversarial patches for object detection," *arXiv preprint arXiv:1906.11897*, 2019.

[6] K. Xu, G. Zhang, S. Liu, Q. Fan, M. Sun, H. Chen, P.-Y. Chen, Y. Wang, and X. Lin, "Adversarial t-shirt! evading person detectors in a physical world," in *European Conference on Computer Vision (ECCV)*, 2020, pp. 665–681.

[7] Z.-Q. Zhao, P. Zheng, S.-T. Xu, and X. Wu, "Object detection with deep learning: A review," *IEEE Transactions on Neural Networks and Learning Systems*, vol. 30, no. 11, pp. 3212–3232, 2019.

[8] J. Redmon, S. Divvala, R. Girshick, and A. Farhadi, "You only look once: Unified, real-time object detection," in *IEEE Conference on Computer Vision and Pattern Recognition (CVPR)*, 2016, pp. 779–788.

[9] J. Redmon and A. Farhadi, "Yolov3: An incremental improvement," *arXiv preprint arXiv:1804.02767*, 2018.

[10] A. Bochkovskiy, C.-Y. Wang, and H.-Y. M. Liao, "Yolov4: Optimal speed and accuracy of object detection," *arXiv preprint arXiv:2004.10934*, 2020.

[11] W. Liu, D. Anguelov, D. Erhan, C. Szegedy, S. Reed, C.-Y. Fu, and A. C. Berg, "Ssd: Single shot multibox detector," in *European Conference on Computer Vision (ECCV)*, 2016, pp. 21–37.

[12] S. Ren, K. He, R. Girshick, and J. Sun, "Faster r-cnn: Towards real-time object detection with region proposal networks," *Advances in neural information processing systems*, vol. 28, 2015.

[13] K. He, G. Gkioxari, P. Dollár, and R. Girshick, "Mask r-cnn," in *IEEE International Conference on Computer Vision (ICCV)*, 2017, pp. 2961–2969.

[14] S.-M. Moosavi-Dezfooli, A. Fawzi, O. Fawzi, and P. Frossard, "Universal adversarial perturbations," in *IEEE Conference on Computer Vision and Pattern Recognition (CVPR)*, 2017, pp. 1765–1773.

[15] R. Gurbaxani and S. Mishra, "Traits & transferability of adversarial examples against instance segmentation & object detection," *arXiv preprint arXiv:1808.01452*, 2018.

[16] K.-H. Chow, L. Liu, M. Loper, J. Bae, M. E. Gursoy, S. Truex, W. Wei, and Y. Wu, "Adversarial objectness gradient attacks in real-time object detection systems," in *IEEE International Conference on Trust, Privacy and Security in Intelligent Systems and Applications (TPS-ISA)*, 2020, pp. 263–272.

[17] D. Li, J. Zhang, and K. Huang, "Universal adversarial perturbations against object detection," *Pattern Recognition*, vol. 110, p. 107584, 2021.

[18] O. M. Nezami, A. Chaturvedi, M. Dras, and U. Garain, "Pick-object-attack: Type-specific adversarial attack for object detection," *Computer Vision and Image Understanding*, vol. 211, p. 103257, 2021.

[19] C. Xie, J. Wang, Z. Zhang, Y. Zhou, L. Xie, and A. Yuille, "Adversarial examples for semantic segmentation and object detection," in *IEEE International Conference on Computer Vision (ICCV)*, 2017, pp. 1369–1378.

[20] A. S. Hashemi, A. Bär, S. Mozaffari, and T. Fingscheidt, "Transferable universal adversarial perturbations using generative models," *arXiv preprint arXiv:2010.14919*, 2020.

[21] X. Wei, S. Liang, N. Chen, and X. Cao, "Transferable adversarial attacks for image and video object detection," in *International Joint Conference on Artificial Intelligence (IJCAI)*, 2019, pp. 954–960.

[22] N. Carlini and D. Wagner, "Towards evaluating the robustness of neural networks," in *IEEE Symposium on Security and Privacy*, 2017, pp. 39–57.

[23] Q. Liao, X. Wang, B. Kong, S. Lyu, B. Zhu, Y. Yin, Q. Song, and X. Wu, "Transferable adversarial examples for anchor free object detection," in *IEEE International Conference on Multimedia and Expo (ICME)*, 2021, pp. 1–6.

[24] N. Bodla, B. Singh, R. Chellappa, and L. S. Davis, "Soft-nms improving object detection with one line of code," in *IEEE International Conference on Computer Vision (ICCV)*, 2017, pp. 5561–5569.

[25] A. Madry, A. Makelov, L. Schmidt, D. Tsipras, and A. Vladu, "Towards deep learning models resistant to adversarial attacks," *arXiv preprint arXiv:1706.06083*, 2017.

[26] M. Everingham, L. Van Gool, C. K. I. Williams, J. Winn, and A. Zisserman, "The PASCAL Visual Object Classes Challenge 2012 (VOC2012)," 2012. [Online]. Available: http://www.pascal-network.org/challenges/VOC/voc2012/workshop/index.html

[27] J. Cartucho, R. Ventura, and M. Veloso, "Robust object recognition through symbiotic deep learning in mobile robots," in *IEEE International Conference on Intelligent Robots and Systems (IROS)*, 2018, pp. 2336–2341.

[28] V. Fischer, M. C. Kumar, J. H. Metzen, and T. Brox, "Adversarial examples for semantic image segmentation," in *International Conference on Learning Representations (ICLR)*, 2017.